

Crystal and electronic structure of a quasi-two-dimensional semiconductor $\text{Mg}_3\text{Si}_2\text{Te}_6$

Chaoxin Huang,^{1,*} Benyuan Cheng,^{2,3,*} Yunwei Zhang,¹ Long Jiang,⁴ Lisi Li,¹ Mengwu Huo,¹ Hui Liu,¹ Xing Huang,¹ Feixiang Liang,¹ Lan Chen,¹ Hualei Sun,¹ and Meng Wang^{1,†}

¹Center for Neutron Science and Technology, Guangdong Provincial Key Laboratory of Magnetoelectric Physics and Devices, School of Physics, Sun Yat-Sen University, Guangzhou, 510275, China

²Shanghai Institute of Laser Plasma, Shanghai 201800, China

³Center for High Pressure Science and Technology Advanced Research, Shanghai 201203, China

⁴Instrumentation Analysis and Research Center, Sun Yat-Sen University, Guangzhou 510275, China

We report the synthesis and characterization of a Si-based ternary semiconductor $\text{Mg}_3\text{Si}_2\text{Te}_6$, which exhibits a quasi-two-dimensional structure, where the trigonal $\text{Mg}_2\text{Si}_2\text{Te}_6$ layers are separated by Mg ions. Ultraviolet-visible absorption spectroscopy and density functional theory calculations were performed to investigate the electronic structure. The experimentally determined direct band gap is 1.39 eV, consistent with the value of the density function theory calculations. Our results reveal that $\text{Mg}_3\text{Si}_2\text{Te}_6$ is a direct gap semiconductor with a relatively narrow gap, which is a potential candidate for infrared optoelectronic devices.

I. INTRODUCTION

Narrow-gap semiconductors (NGS) play an important role in optoelectronic and magnetic devices. Because of their unique advantages, the properties and applications of NGS have been widely studied for decades in a variety of fields, such as magnetic field sensors, photovoltaics, infrared photodetectors, lasers and so on¹⁻⁵. Magnetic field sensors, including magnetoresistors and Hall sensors, are generally used in magnetic recording and magnetic measurement technologies^{6,7}. Materials for magnetic field sensors are doped semiconductors with high electronic density of states and mobility, such as InSb and InAs which are extremely sensitive to magnetic field⁸⁻¹⁰. Conventional photovoltaic materials mostly use wide-gap semiconductors that utilize photons in the ultraviolet and visible regions, limiting the conversion efficiency. Tuning the band gap is considered to be one of the effective solutions¹¹. NGS-based photoelectrodes can absorb light at longer wavelengths and enhance the solar energy conversion efficiency¹². As a more widely used field, infrared photodetectors, such as the quantum dots-in-a-well photodetectors, have developed rapidly in recent years¹³⁻¹⁵. In addition, NGS lasers have attracted more and more attention due to their stability, tunability, simple structure, and many other advantages^{16,17}.

One of the most important parameters for photoelectric materials is the value of the electronic band gap. $\text{Hg}_{1-x}\text{Cd}_x\text{Te}$ and $\text{Pb}_{1-x}\text{Sn}_x\text{Te}$ are among the hottest researched NGS systems in recent years, whose gaps can be tuned by compositions in a wide range, even close to zero¹⁷⁻²⁰. Alloying is also an effective method to modulate the band gap, which is beneficial for the application of the mid- and long-infrared photodetectors²¹. Although InSb and HgCdTe based detectors have been well available in commercial applications, their poor flexibility, instability of the material interface, complex manufacturing process, and low temperature working environment limit their further development²¹⁻²³. Therefore, it is crucial to search for more NGS that are suitable

for manufacturing stable and efficient infrared detectors. Meanwhile, new NGS with excellent performance also have potential applications in laser, photovoltaics, and other magnetic devices.

In this work we report the successful synthesis of a Si-based nonmagnetic semiconductor $\text{Mg}_3\text{Si}_2\text{Te}_6$, whose structure is found to exhibit a quasi-two-dimensional (quasi-2D) layered configuration. Fittings using a direct and indirect band gap models to the ultraviolet-visible (UV-vis) absorption spectra result in a direct gap of 1.39 eV or an indirect gap of 0.6 eV, respectively. Electronic structure calculations using density functional theory (DFT) yield a direct band gap of 1.2 eV, close to the direct gap fitted from the UV-vis absorption spectra, revealing that $\text{Mg}_3\text{Si}_2\text{Te}_6$ is a direct gap semiconductor. The band gap is narrower than the energies of visible photons, allowing $\text{Mg}_3\text{Si}_2\text{Te}_6$ a potential candidate for infrared photoelectric material.

II. EXPERIMENT AND CALCULATION

Single crystal samples of $\text{Mg}_3\text{Si}_2\text{Te}_6$ were grown by a self-flux method²⁴⁻²⁶. Mg (99.99%) robs, Si (99.99%)

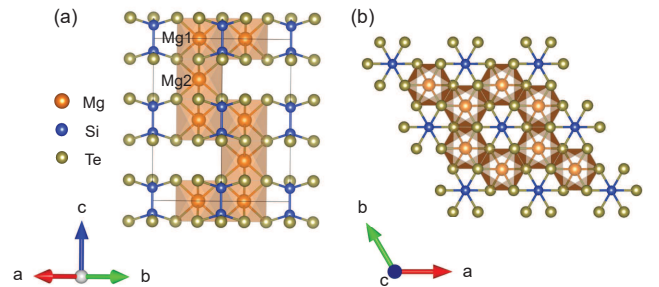


FIG. 1. Crystal structure of $\text{Mg}_3\text{Si}_2\text{Te}_6$ (space group: $P\bar{3}1c$) viewed (a) perpendicular to the c -axis and (b) parallel to the c -axis, respectively. The orange, blue, and grey balls represent Mg, Si, and Te.

TABLE I. Parameters of $\text{Mg}_3\text{Si}_2\text{Te}_6$ refined from single-crystal XRD at 253K.

Empirical formula	$\text{Mg}_3\text{Si}_2\text{Te}_6$
Formula weight	894.69
Temperature	252.99(10) K
Crystal system	trigonal
Space group	$P\bar{3}1c$
Unit-cell parameters	$a = b = 7.0642(9) \text{ \AA}$ $c = 14.464(2) \text{ \AA}$ $\alpha = \beta = 90^\circ$ $\gamma = 120^\circ$
Atomic parameters	
Mg1	4f (1/3, 2/3, 0.4987(5))
Mg2	2d (2/3, 4/3, 1/4)
Si	4e (0, 1, 0.4192(4))
Te	12i (x, y, z) $x = 0.3402(1), y = 0.9990(2),$ $z = 0.3733(1)$
Volume	$625.11(18) \text{ \AA}^3$
Density	4.753 g/cm^3
Absorp. coeff.	14.102 mm^{-1}
$F(000)$	725.0
Crystal size	$0.09 \times 0.04 \times 0.02 \text{ mm}^3$
Radiation	Mo K_α ($\lambda = 0.7107 \text{ \AA}$)
2θ range for data collection	5.632° to 53.96°
Index ranges	$-9 \leq h \leq 7, -9 \leq k \leq 9,$ $-18 \leq l \leq 18$
Reflections collected	3733
Independent reflections	439
Data/restraints/parameters	439/0/18
Goodness-of-fit on F^2	0.904
Final R indexes [$I \geq 2\sigma(I)$]	$R_1 = 0.0391, wR_2 = 0.0790$
Final R indexes [all data]	$R_1 = 0.0767, wR_2 = 0.1014$
Largest diff. peak/hole/ $e \text{ \AA}^{-3}$	1.38/ - 0.96

powders, and Te blocks (99.99%) were mixed in a molar ratio of 3 : 2 : 6 after rough grinding, then sealed in an evacuated quartz ampoule. The ampoule was firstly heated to 600 °C in 10 h and held for 15 h, then heated to 1050 °C in 20 h and dwelled for 10 h, followed by a slow cooling to 750 °C in 150 h before the furnace was shut down. Shiny plate-like single crystals were obtained. The samples are air sensitive and were stored in an argon-filled glove box to minimize the exposure to air.

Single-crystal x-ray diffraction (XRD) measurements on a single-crystal x-ray diffractometer (SuperNova, Rigaku), a scanning electron microscopy (SEM) photography, and an energy dispersive x-ray spectroscopy (EDS) (EVO, Zeiss) were employed to determine the crystal structure, morphology and composition. Resistivity was measured using the standard four-probe method on single crystals with a typical size of $3 \times 1 \times 0.5 \text{ mm}^3$ on a physical property measurement system (PPMS) (Quantum Design). UV-vis absorption spectroscopy measurements were conducted using an Ocean Optics DH-2000-BAL spectrometer. The sample was pre-peeled into thin flakes with right thickness and then loaded into a diamond anvil cell (DAC) to avoid oxidation. The outboard

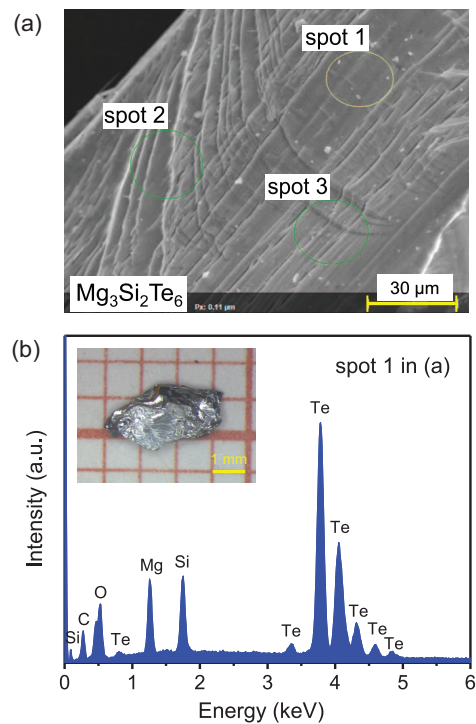


FIG. 2. (a) A zoomed-in view on the surface of the $\text{Mg}_3\text{Si}_2\text{Te}_6$ single crystal taken from SEM. The three circles mark the measured spots. (b) An EDS spectrum of the spot 1 in (a). The elements represented by different characteristic peaks are indicated. Small amounts of carbon and oxygen may derive from the background of conductive adhesive tape. The inset is a photo of the single crystal under an optical microscope.

ring of the DAC is the T301 steel gasket, which was pre-indented and drilled a hole with a diameter of $150 \mu\text{m}$ to serve as the sample chamber. Each spectrum was collected for 2 seconds with wavelenghtes ranged from 180 to 860 nm. The signal from background was obtained by shining the beam on a spot inside the sample chamber but away from the sample.

Electronic band structure was calculated using the DFT within the Perdew-Burke-Ernzerhof (PBE) exchange-correlation as implemented in the Vienna *Ab initio* Simulation Package (VASP) code^{27,28}. A plane wave energy cutoff of 600 eV and dense meshes of Monkhorst-Pack k -points were used to ensure that all calculations are well converged to 1 meV/atom.

III. RESULTS AND DISCUSSION

The structure of $\text{Mg}_3\text{Si}_2\text{Te}_6$ is refined from XRD measurements on single crystals. The structural parameters are summarized in Table I. $\text{Mg}_3\text{Si}_2\text{Te}_6$ crystallizes in the trigonal space group $P\bar{3}1c$ with $a = 7.0642(9) \text{ \AA}$ and $c = 14.464(2) \text{ \AA}$ at 253 K and exhibits a quasi-2D structure. The crystal structures viewed from different

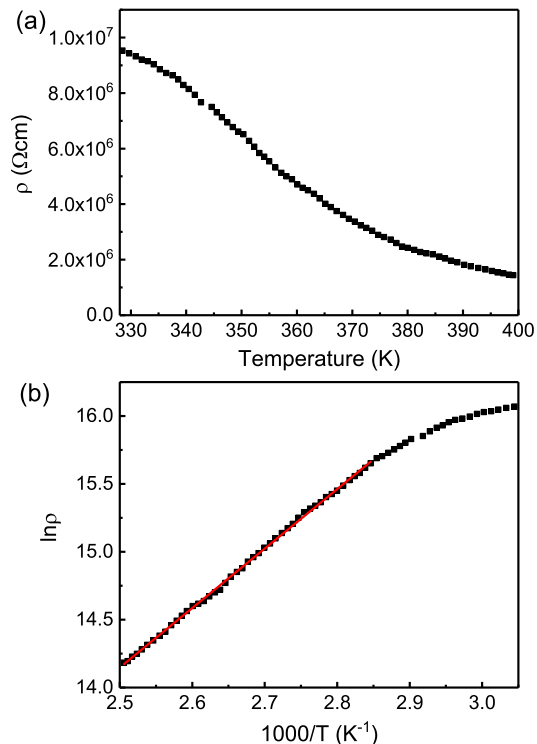


FIG. 3. (a) Resistivity of $\text{Mg}_3\text{Si}_2\text{Te}_6$ in the temperature range of 328~400 K. (b) $\ln \rho$ as a function of $1000/T$. The red line is a fitting using the thermal activation-energy model $\rho(T) = \rho_0 \exp(E_a/k_B T)$.

directions are illustrated in Fig. 1. The layer of the ab plane constituting the formula as $\text{Mg}_2\text{Si}_2\text{Te}_6$ consists of edge shared MgTe_6 octahedra and Si-Si dimers. The $\text{Mg}_2\text{Si}_2\text{Te}_6$ layer is isomorphic to a widely studied 2D van der Waals ferromagnetic compound $\text{Cr}_2\text{Si}_2\text{Te}_6$ ^{29,30}. The layers are linked by Mg2 that is half of Mg1, constituting $\text{Mg}_3\text{Si}_2\text{Te}_6$. $\text{Mg}_3\text{Si}_2\text{Te}_6$ is isostructural to $\text{Mn}_3\text{Si}_2\text{Te}_6$ ³¹ and $\text{Mn}_3\text{Si}_2\text{Se}_6$ ³² which are quasi-2D semiconductors with enriched properties such as ferrimagnetism and large colossal magnetoresistance^{33,34}.

To determine the composition of the samples, we performed EDS measurements on $\text{Mg}_3\text{Si}_2\text{Te}_6$ single crystals. Figure 2(a) is a zoomed-in view of the measured crystal in the ab plane taken from SEM. It is obvious that the crystal is layered with some Te flux on the surface. By normalizing the content of Mg to be 3, the composition determined from EDS is $\text{Mg}_3\text{Si}_{1.87(4)}\text{Te}_{6.8(2)}$. The ratio of Mg to Si ratio is close to expectation. The exceeding content of Te of 13% can be attributed to the excess Te flux on the surface.

Figure 3 shows the resistivity measured between 328 and 400 K. The resistivity below 328 K exceeding 10^6 Ωcm is beyond the measured range of the instrument. As shown in Fig. 3 (a), the resistivity exhibits an insulating behavior, and no obvious anomaly can be observed up to 400 K. Figure 3 (b) is a plot of the resistivity in $\ln \rho$ as a function of $1000/T$. A fitting using the thermal

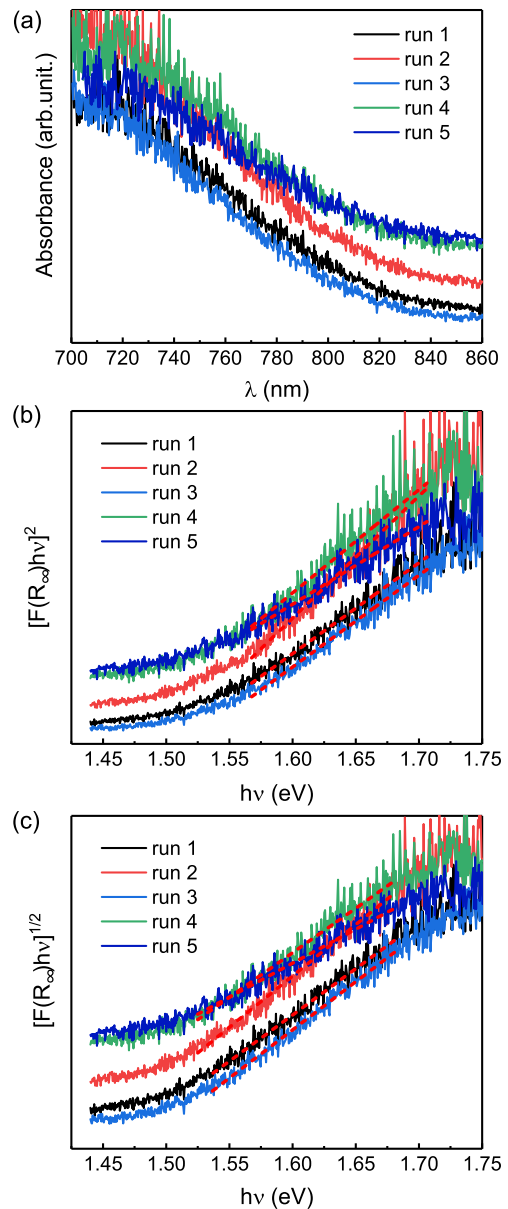


FIG. 4. (a) UV-vis absorption spectra of $\text{Mg}_3\text{Si}_2\text{Te}_6$ in a DAC at room temperature. (b) The Tauc plots of $[F(R_\infty)h\nu]^{1/n} = A(h\nu - E_g)$ versus $h\nu$ with $n = 1/2$ for direct band gap and (c) $n = 2$ for indirect band gap. The dotted red lines are fittings of the linear regions.

activation-energy model $\rho(T) = \rho_0 \exp(E_a/k_B T)$ to the linear segment that corresponds to 350 to 400 K results in $E_a = 0.378$ eV. In the model, ρ_0 is a prefactor, k_B is the Boltzmann constant, and E_a is the thermal activation energy. The obtained activation energy of 0.378 eV indicates that the energy gap of $\text{Mg}_3\text{Si}_2\text{Te}_6$ may be narrower than that of visible light of 1.64 ~ 3.19 eV. We note the fitted thermal activation energy at 350 ~ 400 K may be much smaller than the band gap.

UV-vis absorption spectra were employed to study the electronic band gap of $\text{Mg}_3\text{Si}_2\text{Te}_6$. Five pieces of sin-

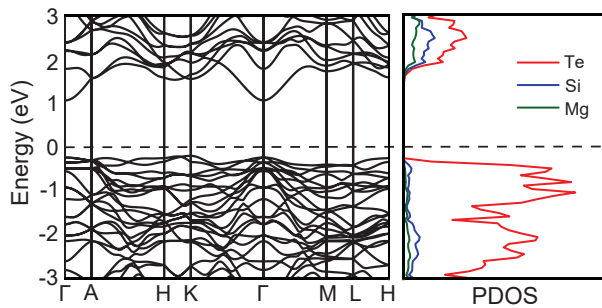


FIG. 5. Electronic structure calculation using DFT. The direct gap of $\text{Mg}_3\text{Si}_2\text{Te}_6$ is about 1.2 eV. PDOS is obtained by integrating density states of the energy bands, and the electrons close to the Fermi surface are mainly provided by Te.

gle crystals were measured separately. The absorption spectra are shown in Fig. 4 (a), yielding a typical semi-conducting state with a strong absorption in the range of 700 ~ 860 nm, while the rest of the short wavelength data are removed because of relatively high noise. The band gap can be obtained by fitting the absorption spectra using the Tauc relation that is $[F(R_\infty)h\nu]^{1/n} = A(h\nu - E_g)$, where $F(R_\infty)$ is the Kubelka-Mubelka-Munk function, h is the Planck constant, ν is the frequency, A is a prefactor, and E_g is the band gap energy³⁵. For a direct band gap semiconductor, n is 1/2; for an indirect band gap semiconductor, n is 2. We plot the Tauc relations as a direct gap and indirect gap semiconductor in Figs. 4 (b) and 4 (c), respectively. The size of the band gap is extracted from the linear regression at the inflection point and the obtained $h\nu$ -intercept value is taken as the band gap value³⁶. The measured absorption spectra could not distinguish the two models due to poor statistic. We fitted the linear parts of five sets of data by adopting the Tauc relation and $n = 1/2$, resulting in the direct band gaps of 1.41, 1.43, 1.43, 1.37, and 1.31 eV. Thus, the direct gap is estimated to be 1.39(5) eV by averaging the fitted values. Following the same procedure and adopting $n = 2$, an indirect band gap of 0.6(2) eV is obtained. The difference in the calculated energy gaps between different data sets can be attributed to the inconsistency of thicknesses of the samples, which causes calculation errors by affecting the transmittance and reflectivity of the samples to ultraviolet light.

In order to distinguish the direct gap and indirect gap from the fittings of the UV-vis absorption spectra, DFT calculations were performed to investigate the electronic band structure. Figure 5 displays the band structures along high symmetry directions in a Brillouin zone and

partial density of states (PDOS) of $\text{Mg}_3\text{Si}_2\text{Te}_6$. The calculated data reveal a direct gap of ~ 1.2 eV at the Γ point, close to the fitting results from the UV-vis absorption spectra using the direct gap model. Thus, $\text{Mg}_3\text{Si}_2\text{Te}_6$ can be considered as a direct gap semiconductor with a gap size of 1.2 ~ 1.39 eV. This value is larger than the thermal activation energy of 0.378 eV fitted from the resistivity between 350 and 400 K. The outcomes may attribute to the fact that the activation energy is fitted from resistance change at high temperature, where thermal fluctuations increase the electron hopping capability, and the gap seems to be narrowed. The direct gap size of $\text{Mg}_3\text{Si}_2\text{Te}_6$ is smaller than the energies of visible light. Through doping, temperature, and pressure, the band gap of $\text{Mg}_3\text{Si}_2\text{Te}_6$ may be further decreased, allowing $\text{Mg}_3\text{Si}_2\text{Te}_6$ one of the potential candidates for infrared photoelectric materials.

IV. SUMMARY

In conclusion, we synthesized single crystals of $\text{Mg}_3\text{Si}_2\text{Te}_6$ by self-flux method, and characterized the structure, composition, resistivity, and electronic band gap. $\text{Mg}_3\text{Si}_2\text{Te}_6$ exhibits a quasi-2D structure constituted by $\text{Mg}_2\text{Si}_2\text{Te}_6$ layers (Mg1) that are linked by Mg2 atoms. The single crystals can be mechanically cleaved and are sensitive to air. By combining the UV-vis absorption spectra and DFT calculations, we demonstrate that $\text{Mg}_3\text{Si}_2\text{Te}_6$ is a direct band gap semiconductor with a gap size of 1.2 ~ 1.39 eV. This gap size is close to that of silicon, and may allow $\text{Mg}_3\text{Si}_2\text{Te}_6$ become one of the candidates for infrared photoelectric or other functional materials by tuning the energy level by rare earth ions doping. Moreover, the direct gap characteristics may provide higher photon absorption efficiency compared with traditional indirect-gap Si-based semiconductors. The absorption capacity and conversion efficiency require further investigations.

V. ACKNOWLEDGMENTS

Work was supported by the National Natural Science Foundation of China (Grants No. 12174454, No. 11904414, No. 11904416, and No. 12104427), the Guangdong Basic and Applied Basic Research Foundation (Grant No. 2021B1515120015), and National Key Research and Development Program of China (Grant No. 2019YFA0705702).

* The authors contributed equally to this work.

† wangmeng5@mail.sysu.edu.cn

¹ C. T. Elliott, in *Infrared Technology and Applications XXIV*, Vol. 3436 (SPIE, 1998) pp. 763–775.

² H. Maier and J. Hesse, *Organic Crystals, Germanates, Semiconductors*, 145 (1980).

³ R. Stradling, *Brazilian Journal of Physics* **26**, 7 (1996).

- ⁴ L. Xie, J. Wang, J. Li, C. Li, Y. Zhang, B. Zhu, Y. Guo, Z. Wang, and K. Zhang, *Advanced Electronic Materials* **7**, 2000962 (2021).
- ⁵ H. Zhang, H. Liu, K. Wei, O. O. Kurakevych, Y. Le Godec, Z. Liu, J. Martin, M. Guerrette, G. S. Nolas, and T. A. Strobel, *Physical Review Letters* **118**, 146601 (2017).
- ⁶ P. Ripka and M. Janosek, *IEEE Sensors Journal* **10**, 1108 (2010).
- ⁷ J. Heremans, D. Partin, C. Thrush, and L. Green, *Semiconductor Science and Technology* **8**, S424 (1993).
- ⁸ S. Solin, T. Thio, D. Hines, and J. Heremans, *Science* **289**, 1530 (2000).
- ⁹ T. Berus, M. Oszwaldowski, and J. Grabowski, *Sensors and Actuators A: Physical* **116**, 75 (2004).
- ¹⁰ G. Mihajlović, P. Xiong, S. Von Molnár, K. Ohtani, H. Ohno, M. Field, and G. J. Sullivan, *Applied Physics Letters* **87**, 112502 (2005).
- ¹¹ P. Cheng and Y. Yang, *Accounts of Chemical Research* **53**, 1218 (2020).
- ¹² J. Zheng, H. Zhou, Y. Zou, R. Wang, Y. Lyu, S. Wang, *et al.*, *Energy & Environmental Science* **12**, 2345 (2019).
- ¹³ C. Downs and T. E. Vandervelde, *Sensors* **13**, 5054 (2013).
- ¹⁴ P. Martyniuk and A. Rogalski, *Progress in Quantum Electronics* **32**, 89 (2008).
- ¹⁵ W. Chen, Z. Deng, D. Guo, Y. Chen, Y. I. Mazur, Y. Maidaniuk, M. Benamara, G. J. Salamo, H. Liu, J. Wu, *et al.*, *Journal of Lightwave Technology* **36**, 2572 (2018).
- ¹⁶ E. Tournie and A. N. Baranov, *Semiconductors and Semimetals* **86**, 183 (2012).
- ¹⁷ T. Harman and I. Melngailis, in *Applied Solid State Science*, Vol. 4 (Elsevier, 1974) pp. 1–94.
- ¹⁸ A. Rogalski, *Reports on Progress in Physics* **68**, 2267 (2005).
- ¹⁹ W. Lei, J. Antoszewski, and L. Faraone, *Applied Physics Reviews* **2**, 041303 (2015).
- ²⁰ J. Piotrowski and A. Rogalski, *Infrared Physics & Technology* **46**, 115 (2004).
- ²¹ S. Yang, J. Peng, H. Huang, Z. Li, H. Dong, and F. Wu, *Materials Science in Semiconductor Processing* **144**, 106552 (2022).
- ²² J. Piotrowski and A. Rogalski, *Sensors and Actuators A: Physical* **67**, 146 (1998).
- ²³ H. Jiao, X. Wang, Y. Chen, S. Guo, S. Wu, C. Song, S. Huang, X. Huang, X. Tai, T. Lin, *et al.*, *Science Advances* **8**, eabn1811 (2022).
- ²⁴ J. Yin, C. Wu, L. Li, J. Yu, H. Sun, B. Shen, B. A. Frandsen, D.-x. Yao, and M. Wang, *Physical Review Materials* **4**, 013405 (2020).
- ²⁵ H. Sun, C. Chen, Y. Hou, W. Wang, Y. Gong, and M. Huo, *Science China: Physics, Mechanics and Astronomy* **64**, 118211 (2021).
- ²⁶ L. Li, X. Hu, Z. Liu, J. Yu, B. Cheng, S. Deng, L. He, K. Cao, D.-X. Yao, and M. Wang, *Science China: Physics, Mechanics and Astronomy* **64**, 287412 (2021).
- ²⁷ J. P. Perdew, K. Burke, and M. Ernzerhof, *Physical Review Letters* **77**, 3865 (1996).
- ²⁸ R. A. Vargas Hernández, *The Journal of Physical Chemistry A* **124**, 4053 (2020).
- ²⁹ V. Carteaux, D. Brunet, G. Ouvrard, and G. Andre, *Journal of Physics: Condensed Matter* **7**, 69 (1995).
- ³⁰ W. Cai, H. Sun, W. Xia, C. Wu, Y. Liu, H. Liu, Y. Gong, D.-X. Yao, Y. Guo, and M. Wang, *Physical Review B* **102**, 144525 (2020).
- ³¹ H. Vincent, D. Leroux, D. Bijaoui, R. Rimet, and C. Schlenker, *Journal of Solid State Chemistry* **63**, 349 (1986).
- ³² A. F. May, H. Cao, and S. Calder, *Journal of Magnetism and Magnetic Materials* **511**, 166936 (2020).
- ³³ Y. Ni, H. Zhao, Y. Zhang, B. Hu, I. Kimchi, and G. Cao, *Physical Review B* **103**, L161105 (2021).
- ³⁴ J. Seo, C. De, H. Ha, J. E. Lee, S. Park, J. Park, Y. Skourski, E. S. Choi, B. Kim, G. Y. Cho, H. W. Yeom, S.-W. Cheong, J. H. Kim, B.-J. Yang, K. Kim, and J. S. Kim, *Nature* **599**, 576 (2021).
- ³⁵ A. Sarkar, C. Loho, L. Velasco, T. Thomas, S. S. Bhattacharya, H. Hahn, and R. Djenadic, *Dalton Transactions* **46**, 12167 (2017).
- ³⁶ J. Tauc, R. Grigorovici, and A. Vancu, *Physica Status Solidi (b)* **15**, 627 (1966).